ELSEVIER

Chemical Engineering and Processing 42 (2003) 733–742

Chemical Engineering and Processing

www.elsevier.com/locate/cep

Hydrodynamics of internal air-lift reactors: experiments versus CFD simulations

J.M. van Baten, J. Ellenberger, R. Krishna *

Department of Chemical Engineering, University of Amsterdam, Nieuwe Achtergracht 166, 1018 WV Amsterdam, The Netherlands

Received 6 May 2002; received in revised form 28 June 2002; accepted 28 June 2002

Abstract

The hydrodynamics of two configurations of internal airlift reactors, both with a riser diameter of 0.1 m, operating with an air–water system, have been experimentally investigated for a range of superficial gas velocities. The experimental results are compared with a model using Computational fluid dynamics (CFD) with Eulerian descriptions of the gas and liquid phases. Interactions between the bubbles and the liquid are taken into account by means of a momentum exchange, or drag, coefficient based on a literature correlation. The turbulence in the liquid phase is described using the $k-\varepsilon$ model. The CFD model shows excellent agreement with the measured data on gas holdup, liquid velocity in the downcomer and in the riser. The developed CFD model has the potential of being applied as a tool for scaling up.

Keywords: Airlift reactor; Gas hold-up; Scale effects; Computational fluid dynamics (CFD); Liquid circulations

1. Introduction

Airlift reactors (ALR) are finding increasing applications in chemical industry, biochemical fermentation and biological wastewater treatment processes [1–3]. There are two types of ALR, 'internal' and 'external' loop ones. Internal loop reactors consist of concentric tubes or split vessels, in which a part of the gas is entrained into the downcomer, whereas external loop reactors are two conduits connected at the top and the bottom, in which little or no gas recirculates into the downcomer. The part in which the sparger is located is called the riser, and the other one, the downcomer. The driving force, based on the static pressure difference, or the mixture density difference, between the riser and the downcomer generates the loop liquid circulation. Compared with conventional reactors, such as stirred tank reactors or bubble columns, shear stress is relatively constant and mild throughout the reactor.

For design of an airlift reactor, it is necessary to have accurate estimates of the phase holdups and velocities in the riser and downcomer. Several literature studies have focussed on the estimation of these hydrodynamic parameters [2–15]. In particular, the velocities of the liquid in the downcomer and riser are crucially dependent on the frictional losses, which in turn are determined by the geometry of the reactor and the operating conditions. Several empirical correlations have been proposed for the estimation of these hydrodynamic parameters; however, these correlations are restricted in their applicability to the geometry for which they were determined. Extrapolation to other geometries, scales and operating conditions is fraught with uncertainty.

Several recent publications have established the potential of computational fluid dynamics (CFD) for describing the hydrodynamics of bubble columns [16–27]. An important advantage of the CFD approach is that column geometry and scale effects are automatically accounted for. The major objective of the present communication is to develop a CFD model for internal airlift reactors and to test its validity by comparison with experimental data. After checking the ability of the CFD approach to reproduce the measured data, the model is used to predict the influence of geometry and scale on the reactor hydrodynamics.

* Corresponding author. Fax: +31-20-525-5604
E-mail address: krishna@science.uva.nl (R. Krishna).

0255-2701/02/$ - see front matter
PII: S0255-2701(02)00076-4

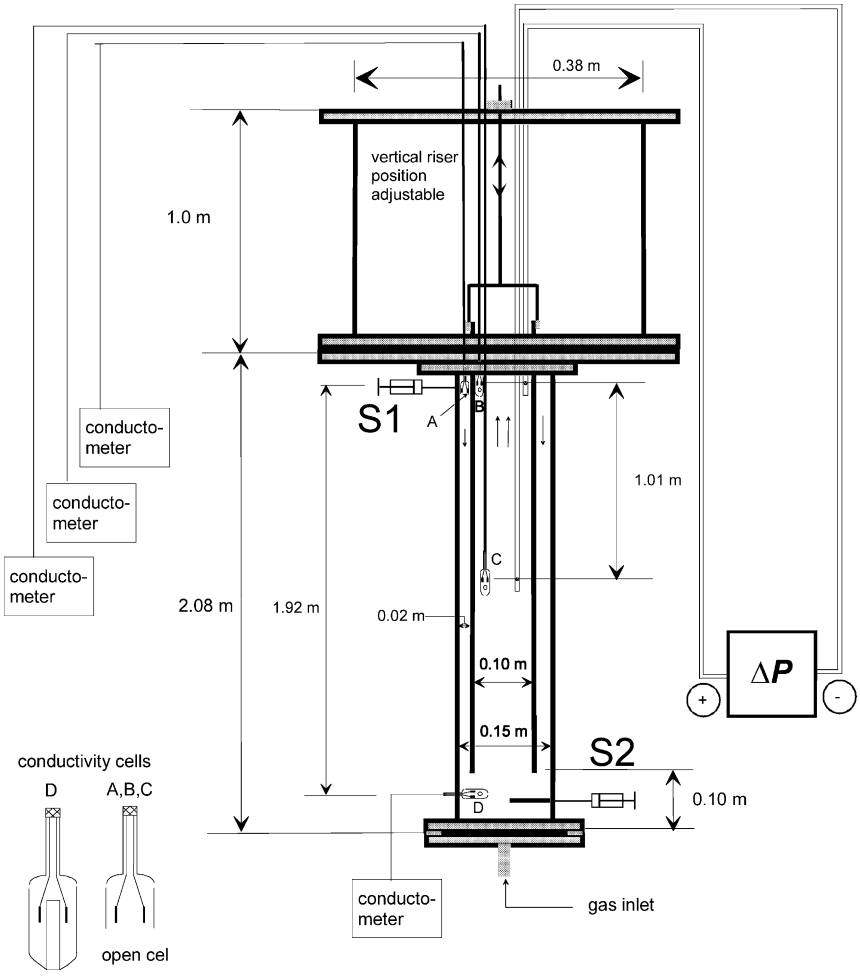

Fig. 1. Experimental set up of internal airlift reactor with Configuration I.

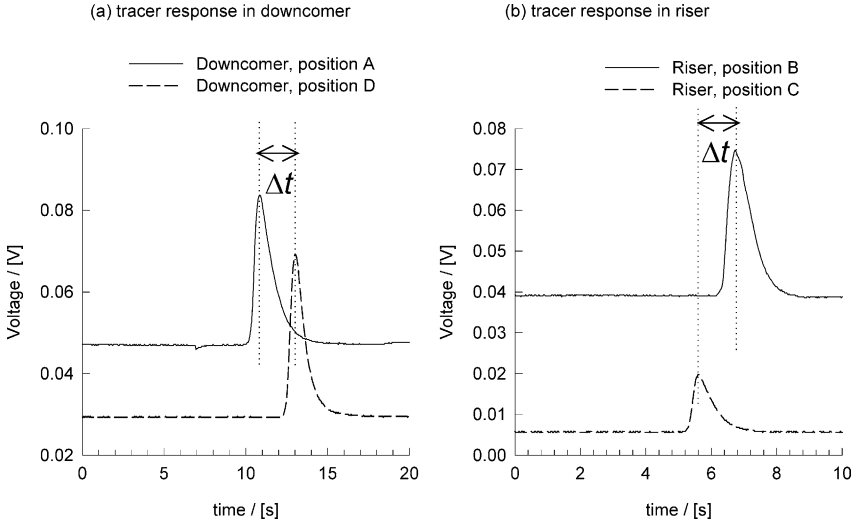

Fig. 2. (a) Voltage responses at positions A and D in the downcomer to salt tracer injection. (b) Voltage responses at positions B and C in the riser to salt tracer injection. Data obtained for Configuration I operating at a superficial gas velocity $U_G = 0.086$ m s^{-1}.

2. Experimental set-up and results

Two configurations of an internal airlift reactor were investigated. Configuration I, shown schematically in Fig. 1, consists of a polyacrylate column with an inner diameter of 0.15 m and a length of 2 m. At the bottom of the column, the gas phase is introduced through a perforated plate with 625 holes of 0.5 mm in diameter. A polyacrylate draft tube (riser) of 0.10 inner and 0.11 m outer diameter with a height of 2.02 m is mounted into the column 0.10 m above the gas distributor. In order to avoid gas flow into the downcomer section, a gas–liquid separator is mounted at the top of the column of 1 m in height and 0.38 m in diameter. In the second configuration II, the same riser of internal diameter was housed in a column of 0.174 m internal diameter; the other dimensions and method of gas distribution were identical to that of Configuration I.

The liquid velocity in the downcomer is determined by injecting, as a pulse, 1 ml of salt tracer (saturated aqueous solution of NaCl) by means of a syringe S1 at a position near the top of the downcomer. The tracer response to this salt tracer injection is measured at two positions, A and D in Fig. 1, by means of conductivity cells (Metrohm) placed near the top and bottom of the downcomer, separated by a distance of 1.92 m. The conductivity cells are connected to a Consort K920 portable conductivity meter, and the transient voltage signals are recorded continuously on a PC. Typical response signals in the downcomer are shown in Fig. 2(a). From the delay in the responses, Δt, the downcomer liquid velocity is determined from $1.92/\Delta t$.

For determination of the liquid velocity in the riser, 1 ml of saturated aqueous solution NaCl is injected as a pulse near the bottom of the riser in the central region through a 1 mm stainless steel capillary by means of a syringe S2. The response is monitored by two conductivity probes at positions C and D, separated by a distance of 1.01 m. Typical response signals in the riser are shown in Fig. 2(b). From the delay in the responses, Δt, the liquid velocity in the riser is determined from $1.01/\Delta t$.

The gas holdup in the riser section is determined by pressure drop measurement between the same two positions, B and C, as indicated for the conductivity cells. Two closed-end stainless steel tubes with a hole of 1.0 mm facing at a right angle to the flow direction are fixed into the riser section, the distance between the holes being 1.0 m. The pressure is transmitted through these tubes to a Validyne DP 15 pressure transducer with a range of 0–2200 Pa. The measuring time of the pressure signal is 120 s with a sampling frequency of 2 Hz. The mean value of the pressure drop signals is used to calculate the gas holdup.

All experiments were carried out at atmospheric pressure conditions with the air–water system. The column is filled with demineralised water to a height of 2.5 m. The hydrodynamics of the airlift system was studied for superficial gas velocities, U_G (based on the 0.1 m diameter riser cross-section) in the range 0.01–0.12 m s^{-1}. For this range of U_G values, there was no entrainment of gas in the downcomer.

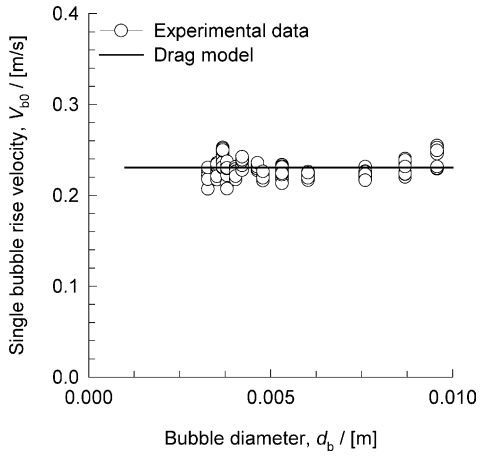

Fig. 3. Experimental data on single bubble rise velocity as a function of bubble diameter [29], compared with predictions of the drag model adopted in this work.

3. Development of CFD model

For either gas or liquid phase the volume-averaged mass and momentum conservation equations in the Eulerian framework are given by:

$$\frac{\partial(\varepsilon_k\rho_k)}{\partial t} + \nabla(\rho_k\varepsilon_k u_k) = 0 \quad (1)$$

$$\frac{\partial(\rho_k\varepsilon_k\mathbf{u}_k)}{\partial t} + \nabla(\rho_k\varepsilon_k\mathbf{u}_k\mathbf{u}_k - \mu_k\varepsilon_k(\nabla\mathbf{u}_k + (\nabla\mathbf{u}_k)^T)) = -\varepsilon_k\nabla p + \mathbf{M}_{kl} + \rho_k\mathbf{g} \quad (2)$$

where, ρ_k, $\mathbf{u}_k$, ε_k and μ_k represent, respectively, the macroscopic density, velocity, volume fraction and viscosity of phase k, p is the pressure, $\mathbf{M}_{kl}$, the interphase momentum exchange between phase k and phase l and g is the gravitational force.

The momentum exchange between the gas (subscript G) and liquid (subscript L) phases is given by:

$$\mathbf{M}_{L,G} = \left[\frac{3}{4}\frac{C_D}{d_b}\rho_L\right]\varepsilon_G(\mathbf{u}_G - \mathbf{u}_L)|\mathbf{u}_G - \mathbf{u}_L| \quad (3)$$

here, the interphase drag coefficient is calculated from [28]:

$$C_D = \frac{2}{3}\sqrt{E\ddot{o}} \quad (4)$$

with:

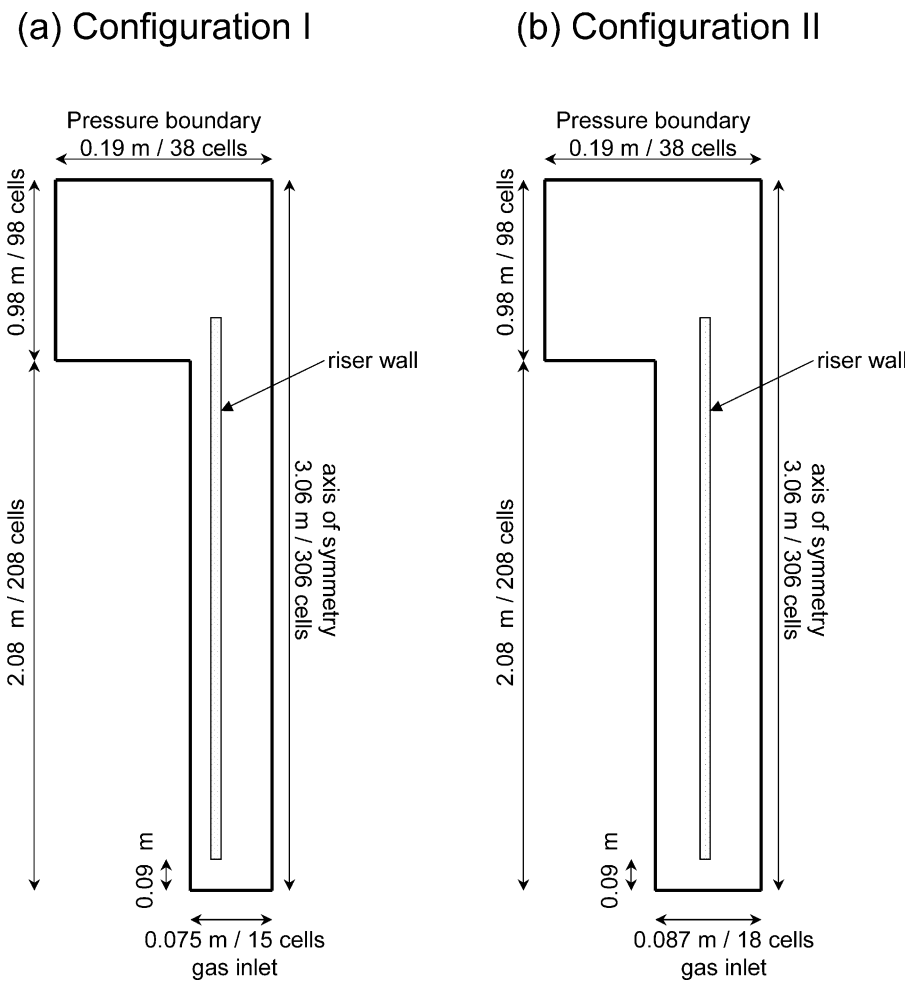

Fig. 4. Computational grid details for Configurations I and II.

$$E = \frac{d(\rho_L - \rho_G)d_b^2}{\sigma} \quad (5)$$

where, d_b is the equivalent diameter of the bubbles. For a single bubble rising in a quiescent liquid, the rise velocity V_{b0} can be calculated from the drag coefficient:

$$V_{b0} = \sqrt{\frac{(\rho_L - \rho_G)g}{3/4(C_D/d_b)\rho_L}} \quad (6)$$

The calculations of the single bubble rise velocity V_{b0} using Eqs. (4)–(6) compare very well with the rise velocity of single air bubbles in water in a column of 0.1 m diameter [29]; see Fig. 3. We note that the rise velocity is practically independent of the bubble size in the 3–8 mm range. For the simulations reported here, we choose a bubble diameter $d_b = 5$ mm.

We have only included the drag force contribution to $\mathbf{M}_{L,G}$, in keeping with the works of Sanyal et al. [18] and Sokolichin and Eigenberger [19]. The added mass and lift force contributions were both ignored in the present analysis.

For the continuous, liquid, phase, the turbulent contribution to the stress tensor is evaluated by means of k–ε model, using standard single-phase parameters $C_\mu = 0.09$, $C_{1\varepsilon} = 1.44$, $C_{2\varepsilon} = 1.92$, $\sigma_k = 1$ and $\sigma_\varepsilon = 1.3$. The applicability of the k–ε model has been considered in detail by Sokolichin and Eigenberger [19]. No turbulence model is used for calculating the velocity fields inside the dispersed bubble phases.

A commercial CFD package CFX, versions 4.2 and 4.4, of AEA Technology, Harwell, UK, was used to solve the equations of continuity and momentum. This package is a finite volume solver, using body-fitted grids. The grids are non-staggered and all variables are evaluated at the cell centres. An improved version of the Rhie–Chow algorithm [30] is used to calculate the velocity at the cell faces. The pressure-velocity coupling is obtained using the SIMPLEC algorithm [31]. For the convective terms in Eqs. (1) and (2), hybrid differencing was used. A fully implicit backward differencing scheme was used for the time integration.

Most of the simulations were carried out using axi-symmetric 2D grids. The grid is shown in Fig. 4 for

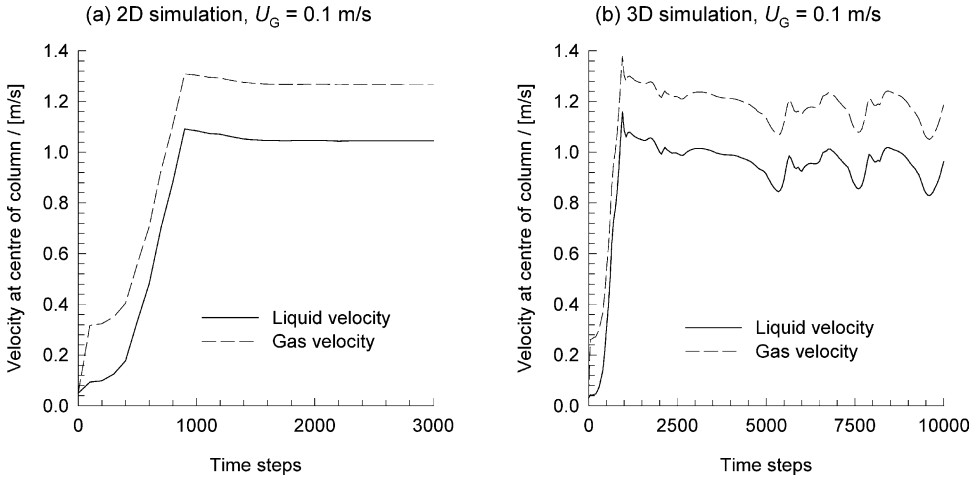

Fig. 5. Transient approach to steady state of velocities and gas holdup in the riser. Simulation results for Configuration I operating at a superficial gas velocity $U_G = 0.10$ m s^{-1} in the riser, at a height of 1.75 m above the distributor. (a) 2D axi-symmetric simulation, and (b) 3D simulation. Animations can be viewed on the web-site: http://ct-cr4.chem.uva.nl/airlift/.

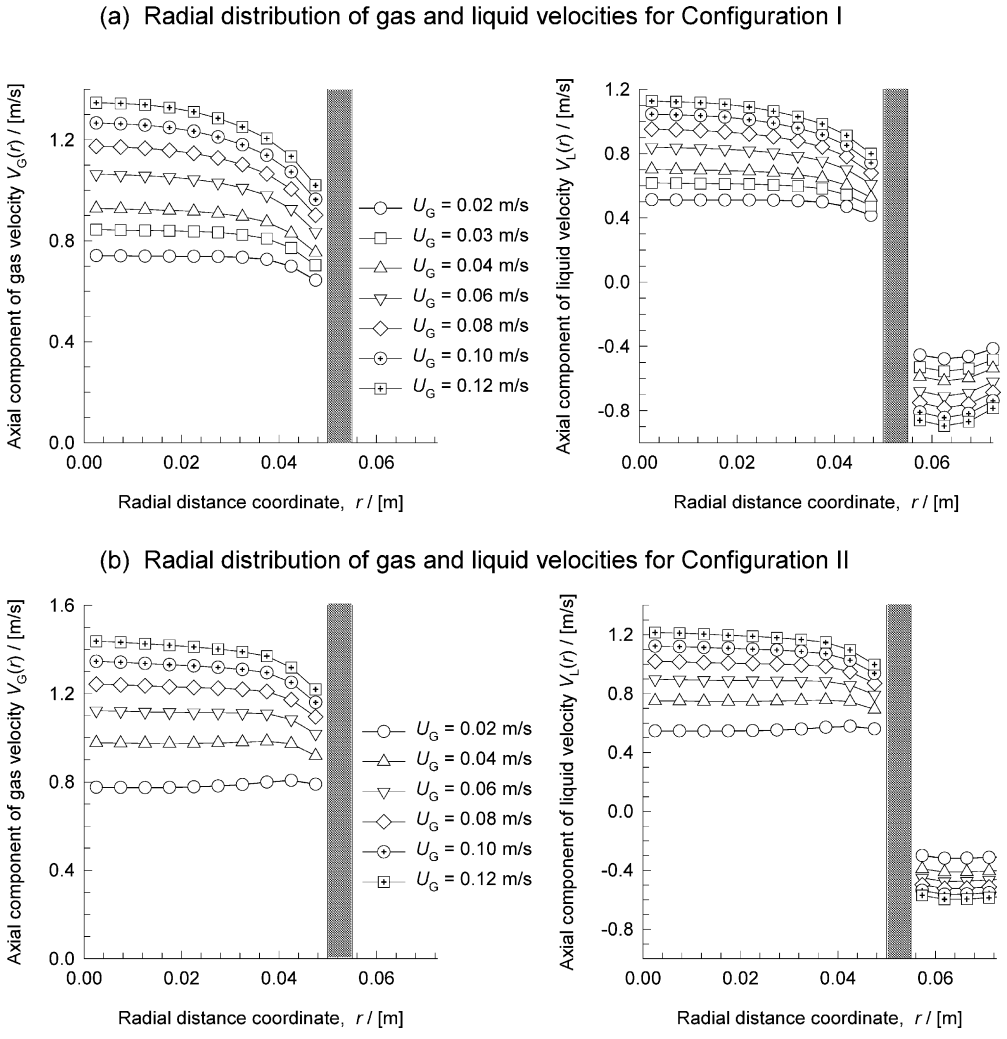

Fig. 6. Radial distribution of gas velocity $V_G(r)$ and liquid velocity $V_L(r)$ for varying superficial gas velocities U_G in the riser, at a height of 1.75 m above the distributor. Two-dimensional axi-symmetric simulation results for Configurations I and II.

Configurations I and II. In the radius of the smaller part of the column, 15 equally spaced cells of 0.005 m are present. In the larger radius of the column, 38 equally spaced cells of 0.005 m are present. The draft tube (riser wall) starts at 0.09 m above the distributor, and ends 2.11 m above the distributor. The outer diameter of the riser is 0.1 m. The inner diameter of the downcomer is 0.11 m. The downcomer wall has a thickness of 0.005 m. The downcomer itself is 0.02 m wide. The total number of cells for Configuration I and II are 6844 and 7468, respectively.

The gas was injected homogeneously over the complete bottom region (over an area equivalent to the sum of the cross-sectional areas of the riser, the downcomer and the draft tube). A pressure boundary condition was applied to the top of the column. A standard no-slip boundary condition was applied at all walls. The time stepping strategy used in all simulations was 100 steps at 5×10^{-5} s, 100 steps at 1×10^{-4} s, 100 steps at 5×10^{-4} s, 100 steps at 1×10^{-3} s, 200 steps at 3×10^{-3} s, 1400 steps at 5×10^{-3} s, and 1000 steps at 1×10^{-2} s. This is more than sufficient to reach steady state, which was indicated by a situation in which all of the variables remained constant. To prevent start-up problems, the system was initialised by setting the gas holdup within the riser to 10%, and setting an initial upward velocity of 0.05 m s^{-1} in the riser, and a matching downward velocity in the downcomer.

The simulations were carried out on Silicon Graphics Power Indigo workstations with 75 MHz R8000 processors, a Silicon Graphics O_2 workstation with a 150 MHz R10000 processor, and a WINDOWS NT PC with a single Pentium Celeron processor running at 500 MHz. Each simulation was completed in about 2 days. Further details of the simulations are available on our web site: http://ct-cr4.chem.uva.nl/airlift/.

In order to test the validity of the assumption of 2D axi-symmetry, one fully three-dimensional simulation was carried out for Configuration I operating $U_G = 0.10$ m s^{-1}. The 3D grid consisted of a total of 68 440 cells, with ten cells in the azimuthal direction. The 3D simulation was carried out on a Silicon Graphics Power Challenge machine employing six R10000 processors in parallel; this simulation took 7 days to complete 10 000 time steps.

4. Simulation results and comparison with experiments

A typical transient approach to steady-state of the gas and liquid velocities, at the centre of the column, are shown in Fig. 5 for Configuration I operating at a superficial gas velocity $U_G = 0.1$ m s^{-1}. Fig. 5(a) shows that the 2D axi-symmetric simulation reaches steady state within 2000 time steps. The steady-state values of all the hydrodynamic parameters were determined at a position 1.75 m above the distributor and reported below. The transient behaviour of the corresponding 3D simulation shows that quasi-steady state is achieved after 5000 time steps; see Fig. 5(b). For the 3D simulation results, time averaged values for 5000–10 000 time step interval are reported below.

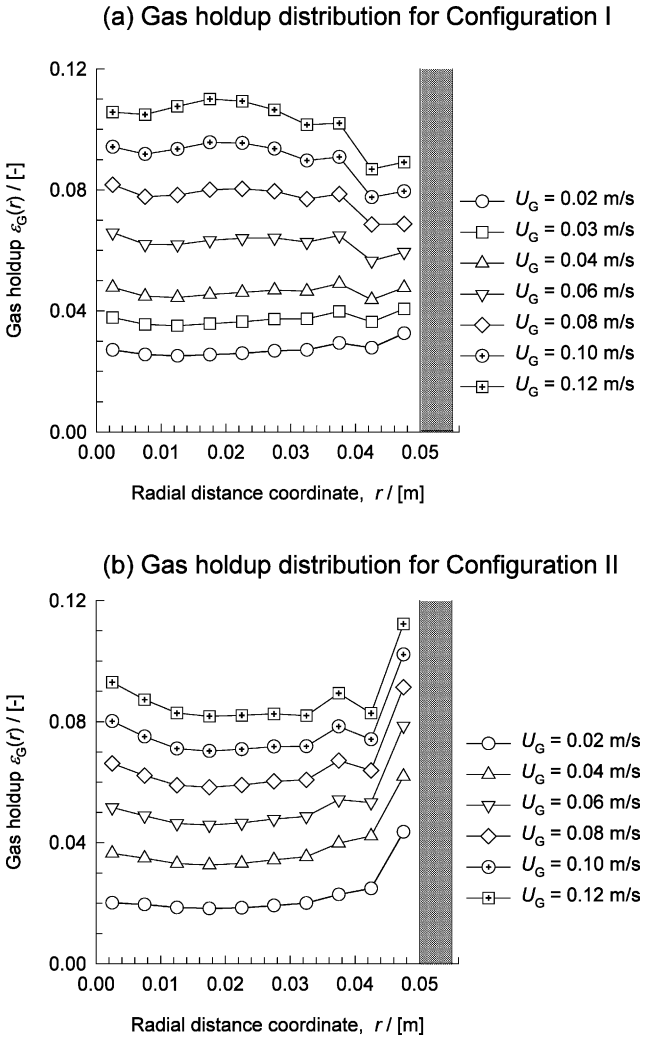

Fig. 7. Radial distribution of gas holdup $\varepsilon_G(r)$ for varying superficial gas velocities U_G in the riser, at a height of 1.75 m above the distributor. Two-dimensional axi-symmetric simulation results for Configurations I and II.

The steady-state radial velocity profiles, from 2D simulations, of the gas and liquid phases are shown in Fig. 6 for Configurations I and II. For low superficial gas velocities, U_G, both gas and liquid phase can be considered to be virtually in plug flow. With increasing superficial gas velocities, both gas and liquid phases lose their plug flow character and the velocity profiles assume a parabolic shape.

The radial distribution of gas holdup, obtained from 2D simulations for Configurations I and II are shown in Fig. 7. Within the central core of the riser, the gas

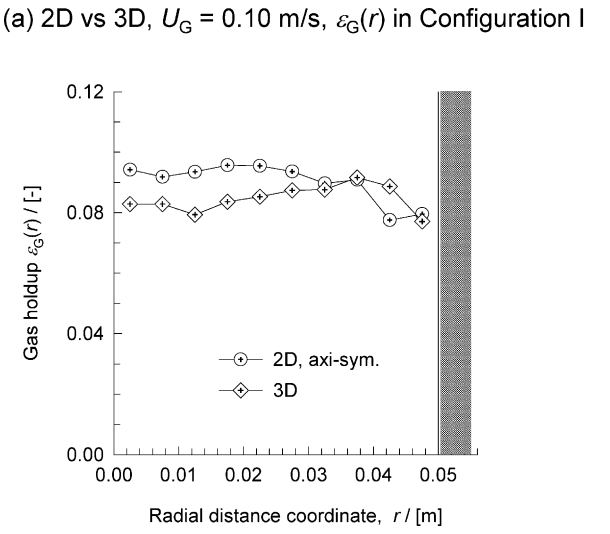

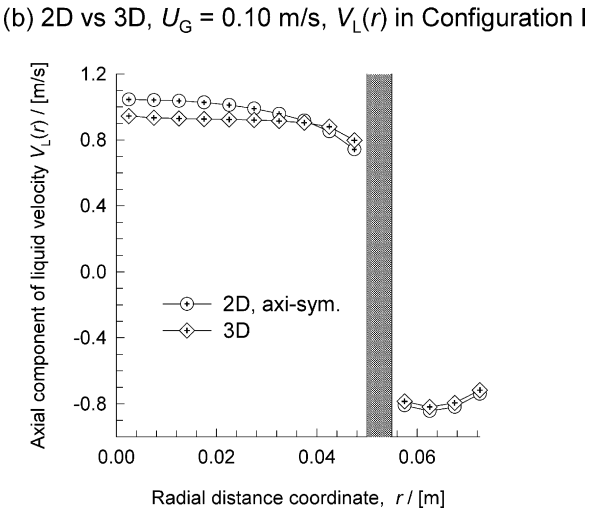

Fig. 8. Comparison of 2D axi-symmetric and 3D simulation results for (a) radial distribution of gas holdup $\varepsilon_G(r)$ and (b) radial distribution of liquid velocity $V_L(r)$. Data at a height of 1.75 m above the distributor. Simulation results for Configuration I operating at a superficial gas velocity $U_G = 0.10$ m s^{-1} in the riser. Animations can be viewed on the

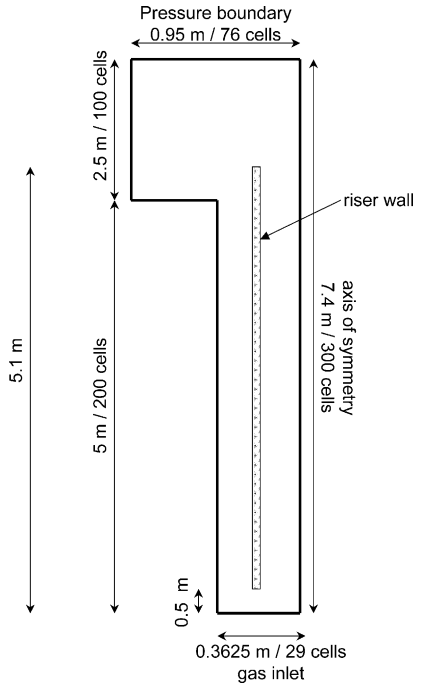

Fig. 10. Computational grid details for Configuration III.

holdup profiles are nearly uniform over the complete range of U_G values for either configuration.

In order to check the assumption of axi-symmetry in the 2D simulations reported above, we compare the 2D and 3D simulation results for Configuration I for U_G = 0.1 m s^{-1}; see Fig. 8. Forcing axi-symmetry makes the 2D simulations of the velocity to attain a more parabolic shape. In the 3D simulations, the gas and liquid phase slosh from side to side, as can be evidenced in the animations on our web-site: http://ct-cr4.chem.uva.nl/airlift/. This side-ways sloshing makes the velocity profiles flatter. The cross-section averaged values of the gas holdup and the velocities for the 2D and 3D simulations for Configuration I are, however, nearly equal to each other.

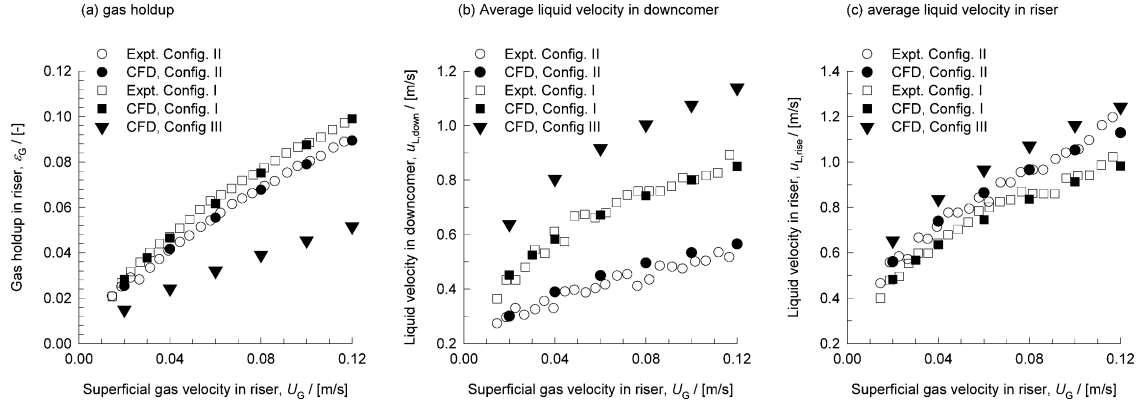

Fig. 9. Comparison of experimental data and simulations for (a) gas holdup in the riser, (b) average liquid velocity in the downcomer and (c) average liquid velocity in the riser.

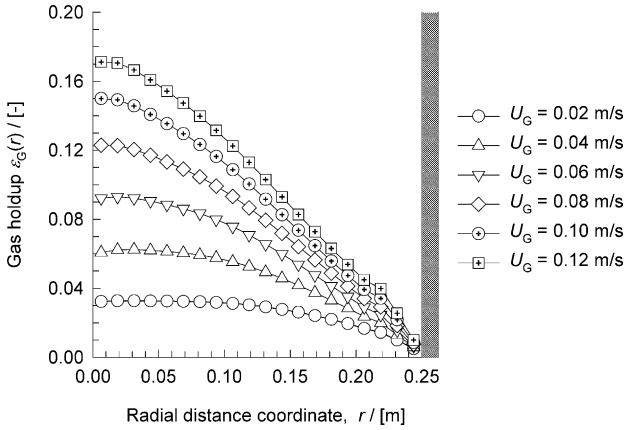

Fig. 11. Radial distribution of gas holdup $\varepsilon_G(r)$ for varying superficial gas velocities U_G in the riser. Two-dimensional axi-symmetric simulation results for Configuration III, at a height of 4.75 m above the gas distributor. Animations can be viewed on the web-site: http://ct-cr4.chem.uva.nl/airlift/.

The cross-section area averaged liquid velocities in the riser and downcomer and gas holdup values in the riser, obtained from the 2D axi-symmetric simulations, are compared in Fig. 9 with the experimentally determined values for configurations I and II.

Configuration II has a larger downcomer area; the frictional losses are smaller and, therefore, a higher volume of liquid is recirculated. The higher liquid recirculations cause a smaller slip velocity between the gas and liquid phases, and consequently a smaller gas holdup. The CFD simulations are able to pick up these geometry effects very well and there is very good agreement with experiments for both Configurations I and II.

5. Scale effects simulated by CFD

In view of the encouraging results obtained above with CFD simulations, we attempted to investigate the influence of scale on the hydrodynamics of internal airlift reactors. For this purpose, we carried out 2D axi-symmetric simulations for a riser of 0.5 m internal diameter. The ratio of the cross-sectional area of the downcomer to that of the riser was maintained the same as for Configuration I. The dimensions of the computational space for the scaled up airlift reactor (called Configuration III) are shown in Fig. 10. A total of grid 13 400 cells was used.

The radial profiles of gas holdup, gas and liquid velocities obtained from 2D axi-symmetric simulations for Configuration III are shown in Figs. 11 and 12. We note that that radial profiles are much more parabolic in shape than for Configurations I and II.

The frictional losses of the liquid phase encountered in Configuration III are much reduced, and this causes much higher liquid re-circulations and a significantly smaller gas holdup; see the results shown in Fig. 9.

6. Conclusions

We have developed a CFD model to describe the hydrodynamics of an internal airlift reactor.

The following major conclusions can be drawn:

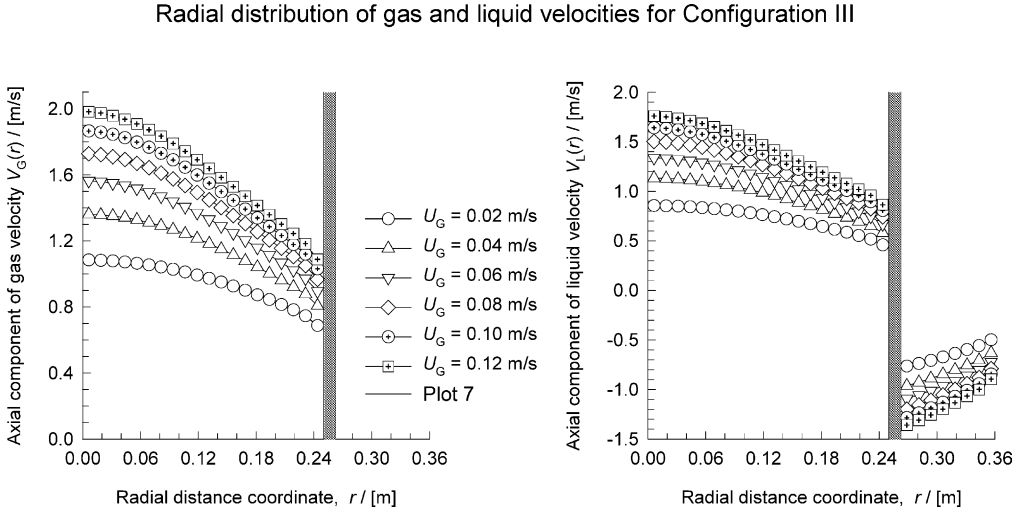

Fig. 12. Radial distribution of gas velocity $V_G(r)$ and liquid velocity $V_L(r)$ for varying superficial gas velocities U_G in the riser. Two-dimensional axi-symmetric simulation results for Configuration III, at a height of 4.75 m above the gas distributor. Animations can be viewed on the web-site: http://ct-cr4.chem.uva.nl/airlift/.

The assumption of 2D axi-symmetry leads to radial profiles of velocity that have a more parabolic character than that for fully 3D simulations.

The cross-section area averaged values of gas holdup and phase velocities for 2D and 3D simulations for Configuration I are close to one another; this result suggests that the assumption of axi-symmetric is valid for the geometry used in the experimental setup.

There is very good agreement between the 2D simulations and experiments for both configurations I and II; this suggests that geometry effects are properly accounted for by the CFD model.

Simulations for a scale up of an airlift reactor (Configuration III) with a riser diameter of 0.5 m, show a significant reduction in the gas holdup due to significantly higher liquid recirculations. This scale up aspect needs to be verified experimentally.

Acknowledgements

The Netherlands Organisation for Scientific Research (NWO) is gratefully acknowledged for providing financial assistance in the form of a 'programmasubsidie' for development of novel concepts in reactive separations technology.

Appendix A: Nomenclature

C_D	drag coefficient, dimensionless
d_b	diameter of bubble (m)
D_T	column diameter (m)
Eö	Eötvös number, $g(\rho_L-\rho_G)d_b^2/\sigma$
g	gravitational acceleration (9.81 m s^{-2})
$\boldsymbol{g}$	gravitational vector (m s^{-2})
M	interphase momentum exchange term (N m^{-3})
p	system pressure (Pa)
r	radial coordinate (m)
t	time (s)
u	velocity vector (m s^{-1})
U_G	superficial gas velocity in the riser (m s^{-1})
$V_b(r)$	radial distribution of bubble velocity (m s^{-1})
$V_L(r)$	radial distribution of liquid velocity, m s^{-1}
V_b	cross-sectional area average rise velocity of bubble swarm (m s^{-1})
V_{b0}	single bubble rise velocity (m s^{-1})

Greek

ε	total gas hold-up, dimensionless
μ	viscosity of fluid phase (Pa s)
ρ	density of phase (kg m^{-3})
σ	surface tension of liquid phase (N m^{-1})

Subscripts

b	referring to bubbles
G	referring to gas
L	referring to liquid
T	tower or column
k,l	referring to phase k and l, respectively
rise	In the riser
down	In the downcomer

References

[1] H. Blenke, Loop reactors, Adv. Biochem. Eng. 13 (1979) 121–215.
[2] M.Y. Chisti, Airlift Bioreactors, Elsevier, London, 1989.
[3] A.E. Saez, M.A. Marquez, G.W. Roberts, R.G. Carbonell, Hydrodynamic model for gas-lift reactors, AIChE J. 44 (1998) 1413–1423.
[4] A.G. Jones, Liquid circulation in a draft-tube bubble column, Chem. Eng. Sci. 40 (1985) 449–462.
[5] E. Garcia-Calvo, P. Leton, Prediction of gas hold-up and liquid velocity in airlift reactors using two-phase flow friction coefficients, J. Chem. Technol. Biotechnol. 67 (1996) 388–396.
[6] J.C. Merchuk, N. Ladwa, A. Cameron, M. Bulmer, I. Berzin, A.M. Pickett, Liquid flow and mixing in concentric tube air-lift reactors, J. Chem. Technol. Biotechnol. 66 (1996) 174–182.
[7] H. Dhaouadi, S. Poncin, J.M. Hornut, G. Wild, P. Oinas, Hydrodynamics of an airlift reactor: experiments and modeling, Chem. Eng. Sci. 51 (1996) 2625–2630.
[8] J.J. Heijnen, J. Hols, R.G.M. van der Lans, H.L.J.M. van Leeuwen, A. Mulder, R. Weltevrede, A simple hydrodynamic model for the liquid circulation velocity in a full scale three phase air lift rector, Chem. Eng. Sci. 52 (1997) 2527–2539.
[9] A. Cockx, A. Line, M. Roustan, Z. Do-Quang, V. Lazarova, Numerical simulation and physical modeling of the hydrodynamics in an air-lift internal loop reactor, Chem. Eng. Sci. 52 (1997) 3787–3793.
[10] W.A.J. Van Benthum, R.G.J.M. van der Lans, M.C.M. van Loosdrecht, J.J. Heijnen, Bubble recirculation regimes in an internal-loop airlift reactor, Chem. Eng. Sci. 54 (1999) 3995–4006.
[11] M.A. Marquez, R.J. Amend, R.G. Carbonell, A.E. Saez, G.W. Roberts, Hydrodynamics of gas-lift reactors with a fast, liquid-phase reaction, Chem. Eng. Sci. 54 (1999) 2263–2271.
[12] K.H. See, G. Roberts, A.E. Saez, Effect of drag and frictional losses on the hydrodynamics of gas-lift reactors, AIChE J. 45 (1999) 2467–2471.
[13] E. Camarasa, E. Carvalho, L.A.C. Meleiro, R. Maciel Filho, A. Domingues, G. Wild, S. Poncin, N. Midoux, J. Bouillard, Development of a complete model for an air-lift reactor, Chem. Eng. Sci. 56 (2001) 493–502.
[14] E. Camarasa, L.A.C. Meleiro, E. Carvalho, A. Domingues, R. Maciel Filho, G. Wild, S. Poncin, N. Midoux, J. Bouillard, A complete model for oxidation air-lift reactors, Comput. Chem. Eng. 25 (2001) 577–584.
[15] R. Oey, R. Mudde, L. Portela, H. Van den Akker, Simulation of a slurry airlift using a two-fluid model, Chem. Eng. Sci. 56 (2001) 673–681.
[16] H.A. Jakobsen, B.H. Sannæs, S. Grevskott, H.F. Svendsen, Modeling of bubble driven vertical flows, Ind. Eng. Chem. Res. 36 (1997) 4052.
[17] Y. Pan, M.P. Dudukovic, M. Chang, Numerical Investigation of Gas-Driven Flow in 2D Bubble Columns, AIChE J. 46 (2000) 434.

[18] J. Sanyal, S. Vasquez, S. Roy, M.P. Dudukovic, Numerical simulation of gas–liquid dynamics in cylindrical bubble column reactors, Chem. Eng. Sci. 54 (1999) 5071.
[19] A. Sokolichin, G. Eigenberger, Applicability of the standard-turbulence model to the dynamic simulation of bubble columns: part I. Detailed numerical simulations, Chem. Eng. Sci. 54 (1999) 2273–2284.
[20] R. Krishna, M.I. Urseanu, J.M. van Baten, J. Ellenberger, Influence of scale on the hydrodynamics of bubble columns operating in the churn-turbulent regime: experiments versus Eulerian simulations, Chem. Eng. Sci. 54 (1999) 4903–4911.
[21] R. Krishna, J.M. van Baten, M.I. Urseanu, Three-phase Eulerian simulations of bubble column reactors operating in the churn-turbulent flow regime: a scale up strategy, Chem. Eng. Sci. 55 (2000) 3275–3286.
[22] R. Krishna, M.I. Urseanu, J.M. van Baten, J. Ellenberger, Liquid phase dispersion in bubble columns operating in the churn-turbulent flow regime, Chem. Eng. J. 78 (2000) 43–51.
[23] R. Krishna, J.M. van Baten, Eulerian simulation of bubble columns operated at elevated pressures in the churn-turbulent regime, Chem. Eng. Sci. 56 (2001) 6249–6258.
[24] R. Krishna, J.M. van Baten, Scaling up bubble column reactors with the aid of CFD, Chem. Eng. Res. Des. Trans. I Chem. E 79 (2001) 283–309.
[25] J.M. Van Baten, R. Krishna, Eulerian simulations for determination of the axial dispersion of liquid and gas phases in bubble columns operating in the churn-turbulent regime, Chem. Eng. Sci. 56 (2001) 503–512.
[26] R. Krishna, J.M. van Baten, M.I. Urseanu, J. Ellenberger, Design and scale-up of the bubble column slurry reactor for Fischer–Tropsch synthesis, Chem. Eng. Sci. 56 (2001) 537–545.
[27] J.B. Joshi, Computational flow modelling and design of bubble column reactors, Chem. Eng. Sci. 56 (2001) 5893–5933.
[28] R. Clift, J.R. Grace, M.E. Weber, Bubbles, Drops and Particles, Academic Press, San Diego, 1978.
[29] R. Krishna, M.I. Urseanu, J.M. van Baten, J. Ellenberger, Wall effects on the rise of single gas bubbles in liquids, Int. Commun. Heat Mass 26 (1999) 781–790.
[30] C.M. Rhie, W.L. Chow, Numerical study of the turbulent flow past an airfoil with trailing edge separation, AIAA J. 21 (1983) 1525–1532.
[31] J. Van Doormal, G.D. Raithby, Enhancement of the SIMPLE method for predicting incompressible flows, Numer. Heat Transfer 7 (1984) 147–163.